Roughness effects on a wall bounded turbulent flow sub-layer

Gaetano Maria Di Cicca [1,*], Michele Onorato [2]

[1] Dipartimento di Ingegneria Meccanica e Aerospaziale, Politecnico di Torino, Turin, Italy
[2] Accademia delle Scienze di Torino, Turin, Italy
*corresponding author: gaetano.dicicca@polito.it

Abstract PIV measurements at relatively low Reynolds numbers in a turbulent boundary layer over a 3D-roughened surface, consisting of pyramidal rows, have been carried out in a closed-loop water tunnel. The ratio between the boundary layer thickness and the pyramidal roughness height is δ/k=17.2 . Measurements have been taken in a streamwise wall normal plane intercepting the apex of a row of pyramids and the diagonal of the square base. The results point out the non-homogeneity of the flow in the roughness sub-layer. The different flow behaviour along the ascendant and the descendent part of the pyramids and in the region between two consecutive pyramids has been visualized. Low values of the streamwise component of the mean velocity and high values of the Reynolds shear stresses are present in the downstream part of the pyramids, near their base. Two series of vortical structures appear to be present in the instantaneous realizations of the flow. Vortices are seen to travel nearly parallel to the wall, very close to the top of the pyramids. It is argued that these vortical structures can be associated with a specific near wall turbulence production mechanism in the roughness sub-layer. Farther from the wall, the instant flow images show vortical structures having a feature similar to the one expected in a smooth wall turbulent boundary layer. Also, a conditional averaged analysis based on the quadrant method has been performed in order to understand the origin of the high turbulence activity observed downstream the pyramids, near their base. Particularly, the flow events producing the high values of the Reynolds shear stress have been analyzed showing that the flow in the roughness sub-layer is strongly influenced by the local wall geometry.

Keywords: Turbulence, wall roughness, boundary layer, PIV.

1 Introduction

Although a large amount of papers has been published on the general subject of a turbulent boundary layer over two and three-dimensional rough surfaces (as a review see [1],[2]), only few results have been published until recently describing the flow in the roughness sub-layer (see e.g. [3],[4],[5],[6]), mostly due to the difficulty of measuring or predicting by numerical simulation flow quantities very near a rough surface [7].

In recent years investigations have been published having as object the study of the flow over pyramidal rough walls. The geometry of this roughness can be simply described in terms of the pyramid's height, orientation with respect to the flow direction, face slope and roughness density. Results of an experimental investigation of the flow over pyramidal rough walls (where both the pyramidal height and the slope were systematically varied) were presented in [8]. The steepest slope of the pyramid surface was 45°, with $\delta/k\cong50$. The Reynolds number, Re_θ , based on the boundary layer momentum thickness, θ , varied from 3960 to 30100. The mean velocity profiles for all the rough surfaces collapse with smooth wall results when presented in velocity defect form, supporting the use of similarity methods. The flow in the roughness sub-layer is not analyzed in the paper. The flow structure and turbulence in a pyramidal rough wall channel flow with $h/k\approx50$, for Re_τ=3520÷5360, were examined in [9]. It was found that the variation, with respect to the canonical case, in the mean flow, Reynolds stresses, turbulent kinetic energy production and dissipation rates are confined to a distance from the wall < $2k$. Instantaneous realizations show that eddies having the same scale of the roughness are generated near the wall and lifted up rapidly by the large-scale structures (hairpin packets) that populate the outer layer. Consequently a small scale roughness signature is present across the entire channel. More recently, paper [7], dealing also with pyramidal roughened wall, focused especially on the turbulence structure and its role in sub-grid-scale energy transfer. To explain the observed flow signature, paper [7] proposed the presence of U-shaped quasi-streamwise vortices developing near the top of the pyramids, as spanwise vorticity is stretched in regions of high streamwise velocity between the pyramidal roughness elements. The flow induced by the adjacent legs of the structures causes powerful ejections that

lift these vortices away from the wall. The existence of these structures has been also supported in [10] by high resolution holographic PIV measurements on a wall roughened by distributed pyramids at Re_τ=3520, h/k = 54.
The cited works having as object the study of the turbulent boundary layer over a pyramidal roughened wall deal with the flow in the roughness sub-layer, showing results from the top of the pyramids up to the external part of the roughness sub-layer.
In the present paper PIV measurements, at relatively low Reynolds numbers, in a turbulent boundary layer over a 3D-roughened surface consisting of pyramidal rows, have been carried out. The ratio between the boundary layer thickness and the pyramidal roughness height is δ/k=17.2 . Measurements have been taken in a streamwise wall normal plane intercepting the apex of a row of pyramids and the diagonal of the square base. The results presented here refer to the flow in the roughness sub-layer including the more internal region close to the base of the pyramids.

2 Experimental setup

The experiments were carried out in a closed-loop water tunnel with a 350 mm wide, 500 mm high, and 1800 mm long test section. Measurements were taken on a flat plate with a length of 2050 mm, in a region about 500 mm downstream the leading edge. The pressure gradient was null along the test section. A three-dimensional roughness (Fig. 1), consisting of pyramids with the diagonal of the square base oriented in the direction of the mean flow, was glued over the surface of the flat plate. The roughness height and geometry were selected to be significant for the case of moderately small values of δ/k. In the present roughness geometry there is a gap g=1.4mm (g/k=0.82) between the pyramid basis.
Measurements were taken with a PIV system, which consisted of a 1280x1024 pixels high speed Dantec NanoSense MKIII CMOS camera and a continuous Spectra-Physics Argon-Ion laser, with a maximum emitted power of 6 W. The laser beam was expanded by a cylindrical lens and focused by a spherical lens, forming a light sheet with a thickness of about 0.5 mm. The water was seeded with spherical silicon carbide particles, 2 μm nominal diameter. PIV measurements were taken in the streamwise wall-normal plane (x,y) intercepting the apex of a row of pyramids and the diagonal of the square base. The physical size of the PIV images was 42x36mm^2 (970x831 viscous units). The PIV images cover the whole boundary layer thickness. The PIV analysis was done with the "LaVision DAVIS 7.2" software to perform the correlations to obtain the velocity fields. The local particle displacements were determined using an adaptive cross-correlation algorithm. The final interrogation window size was 32x32 pixels, overlap of 50%. Each velocity vector is representative of the mean velocity in an area of 1.06x1.06mm^2 (24x24 wall units). The camera acquisition rate was 800 frames per second, but for the statistical analysis only one image pair each 100 frames were recorded. Therefore the effective acquisition rate of PIV image pairs was 8 Hz. 3300 statistically independent image pairs were recorded to ensure the convergence of the computed averaged quantities.

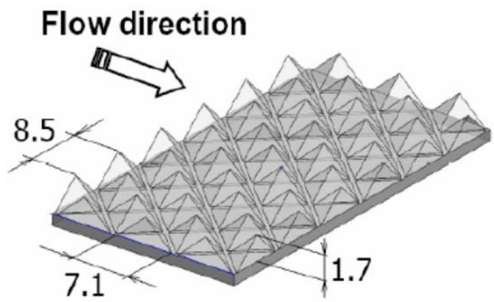

Fig.1 Roughness geometry. Dimensions in millimeters.

3 Results and comments

The experimental test conditions are given in Table 1. The value of the Reynolds number, Re_θ, based on the boundary layer momentum thickness θ and on the external velocity U_e , is 1234. This value characterizes the present results in the range of relatively low Reynolds numbers. The external flow velocity is U_e=0.36m/s. δ is the boundary layer thickness evaluated at $U = 0.99U_e$, where U is the mean velocity. δ was determined taking into account the virtual origin, evaluated according to [11] at 1.27mm below the pyramid top. The ratio between the boundary layer thickness and the roughness height, δ/k=17.2, is in the limit, $16<\delta/k<110$, indicated in [12], in which the outer-layer flow is not influenced by the wall roughness. The friction velocity, U_τ, has been obtained by the modified Clauser chart method [11] applied in the range of the velocity profiles from $y^+\cong60$ to $y/\delta\cong0.23$. The coordinate y is the wall-normal distance from the virtual origin. The apex plus indicates, here and in the following, that the quantity has been normalized with respect to the wall units.

Table 1

U_e	δ	θ	Re_θ	U_τ	U_τ/U_e	k	k^+	δ/k
[m/s]	[mm]	[mm]		[m/s]		[mm]		
0.36	29.29	3.79	1234	0.0255	0.071	1.7	39	17.2

In Figs.2 and 3 the streamwise and the wall-normal components of the mean velocity $\widetilde{U}^+$ and $\widetilde{V}^+$ are visualized in a region covering a wavelength λ_x from the top of one generic pyramid to the top of the next one. The symbol tilde (~) denotes quantities obtained spatially averaging values in corresponding points of each region covering a wavelength λ_x . The coordinate y_T is the wall-normal distance from the top of the pyramids. In both figures 2 and 3, the wall roughness is sketched. The white triangles represent the pyramids highlighted by the laser sheet. The dark triangle represents the row of pyramids standing between the laser sheet and the observation video camera. The flow appears to be quite homogeneous in the streamwise x-direction for $y_T > k$ ($y/\delta > 0.08$), where the streamwise component of the mean velocity shows a quasi constant value along the x-direction, function of the distance from the wall, while the component in the y-direction assumes vanishing values. In the pyramid region the flow is dominated by the geometry of the roughness. Even if the flow field is not completely observable because in part shaded by the row of the dark pyramids sketched in the figures, regions of low values of $\widetilde{U}^+$ are evident downstream the pyramids in the region closer to the their base. This flow clearly contributes to the increased mean drag of the roughened surface with respect to the smooth one. A positive high value of the $\widetilde{V}^+$ component is observed in Fig.3 near the pyramid upstream side (the ascendant part of the pyramid), followed by a negative value in the downstream side (the descendant part of the pyramid).

In Fig.4 the Reynolds shear stresses are displayed. $-\widetilde{<u'v'>}^+$ shows different behaviors in the two sides of the pyramids: higher values in the downstream side, with a peak of $-\widetilde{<u'v'>}^+ \cong 1.6$ and about half of this value in the upstream side. It should be emphasized that downstream the pyramids, in the region between $x/\lambda_x \cong 0.1$ and $x/\lambda_x \cong 0.3$, the Reynolds shear stress assumes a value around 1.5, much higher than the maximum value ($-\widetilde{<u'v'>}^+ = 0.9$) expected near the wall at the same Reynolds number in a smooth wall turbulent boundary layer [13]. In the region between two successive pyramids $-\widetilde{<u'v'>}^+$ also shows a relatively high value, $-\widetilde{<u'v'>}^+ \cong 1$.

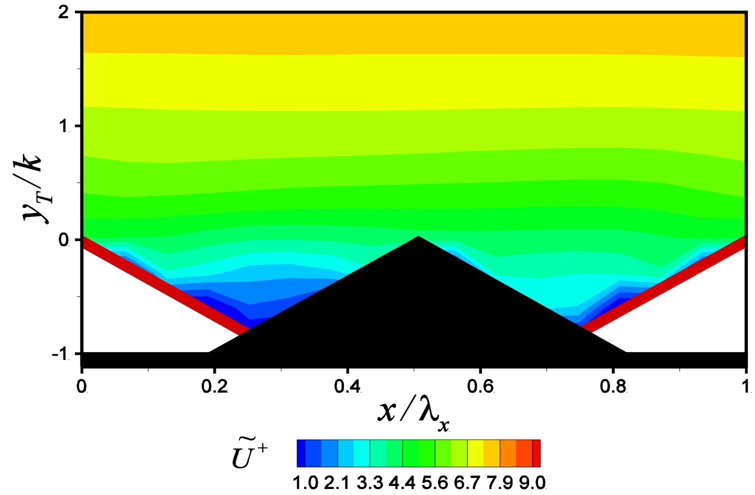

Fig.2 Streamwise component of the mean velocity.

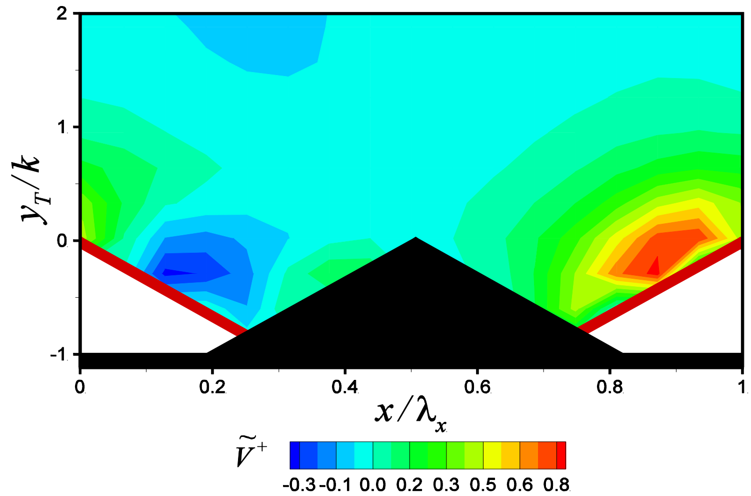

Fig.3 Wall-normal component of the mean velocity.

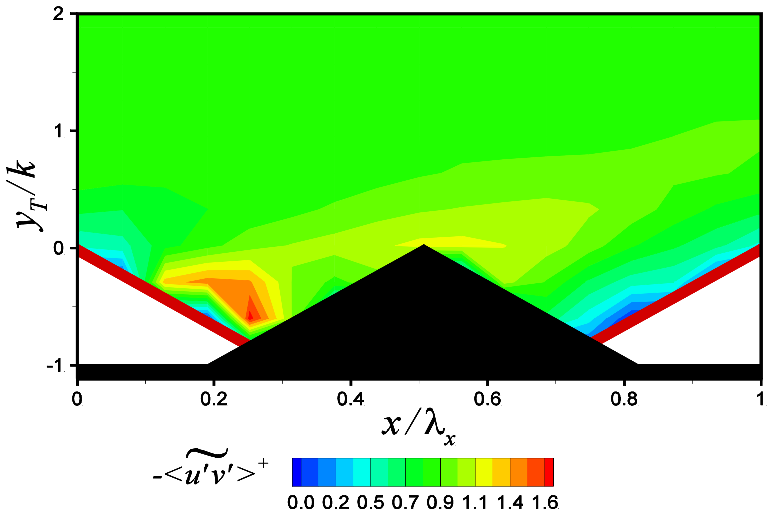

Fig.4 Reynolds shear stresses.

A picture of the instantaneous representation of the flow near the wall is observable in Fig.5, referring to two different instants of the motion. The colour maps represent the instantaneous component of the streamwise velocity while the closed continuous lines represent the swirling strength isolines λ_{ci} = constant. λ_{ci} is defined as the magnitude of the imaginary part of the eigenvalue of the local velocity gradient tensor [14]. Two series of vortical structures appear to be present. Vortices are seen to travel nearly parallel to the wall, very close to the top of the pyramids (Fig.5a). Farther from the wall, the instant flow images in Fig.5a and Fig.5b show vortical structures having a feature similar to the one expected in a smooth wall turbulent boundary layer ([15], [16]). Trains of clockwise swirling motions are seen to travel downstream. They represent the signature in the measurement plane of packets of vortical structures (hairpin vortices and skewed quasi-longitudinal vortices), having an inclination angle similar to the one measured by many authors (see e.g. [17], [18]) in turbulent boundary layers on smooth walls. These packets of vortical structures are situated between zones of nearly constant momentum flow. It has to be expected that the mechanisms of production of these vortices are the same of the ones described for the smooth wall case [14]. Conversely, the origin of the vortex structures near the wall, due to the interaction of the flow with the roughness elements, appears to be specific of the roughness geometry. These near wall vortical structures have been also observed in other experiments. Recently, the developing of *U*-shaped quasi-streamwise vortices near the top of the pyramidal roughness elements, has been proposed ([7], [10]).

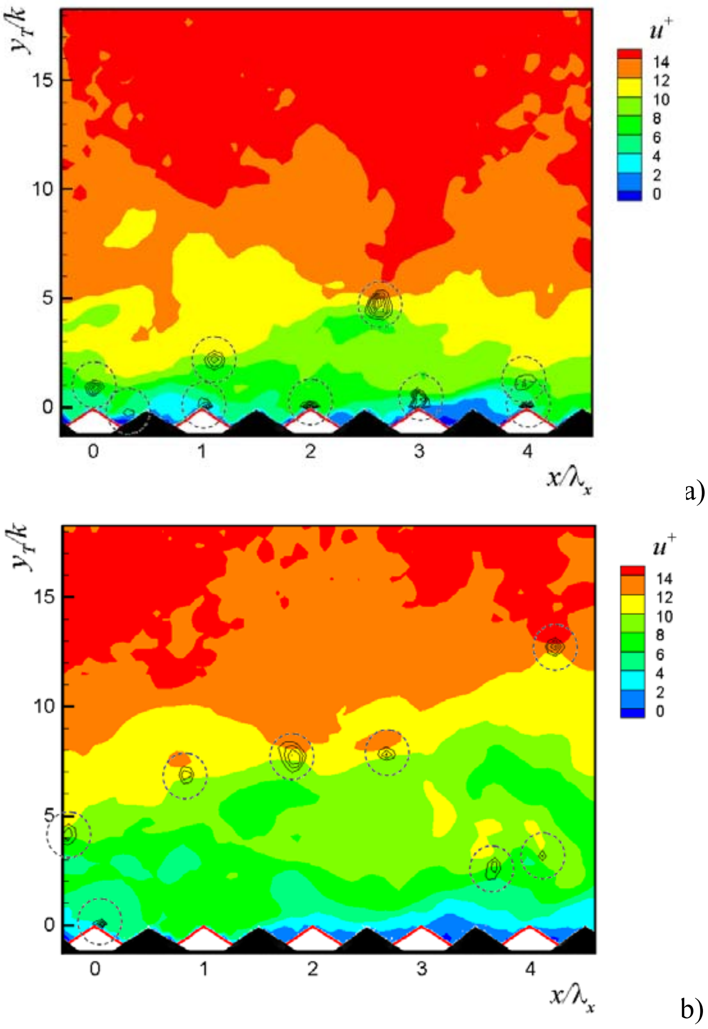

Fig.5 Colour map: instantaneous component of the streamwise velocity. Closed lines: swirling strength isolines. Dashed circles highlight the swirling motions.

The previous results have shown that in the lower part of the inner sub-layer ($y_T < 0$) the major turbulence activity, yielding high values of $-<\widetilde{u'v'}>^+$, holds in the region downstream the pyramids, near their base. In order to understand the origin of the high turbulence activity observed downstream the pyramids, near their base, a quadrant analysis [19] has been performed. In the quadrant method, the local Reynolds shear stress is decomposed into contributions from the four quadrants based on the orientation of the velocity fluctuation vectors: Q1 with $u' > 0$ and $v' > 0$ (outward interaction), Q2 with $u' < 0$ and $v' > 0$ (ejection event), Q3 with $u' < 0$ and $v' < 0$ (inward interaction), Q4 with $u' > 0$ and $v' < 0$ (sweep event). The contribution to the local Reynolds shear stress from a given quadrant, Q, can be expressed as

$$<u'v'>_Q = \lim_{T\to\infty} \frac{1}{T}\int_0^T u'v' I_Q(t)dt$$

where $I_Q(t)$ is a trigger function defined as

$$I_Q = 1 \quad \text{when } |u'v'|_Q \geq H < u'u' >^{1/2} < v'v' >^{1/2}$$
$$I_Q = 0 \quad \text{otherwise}$$

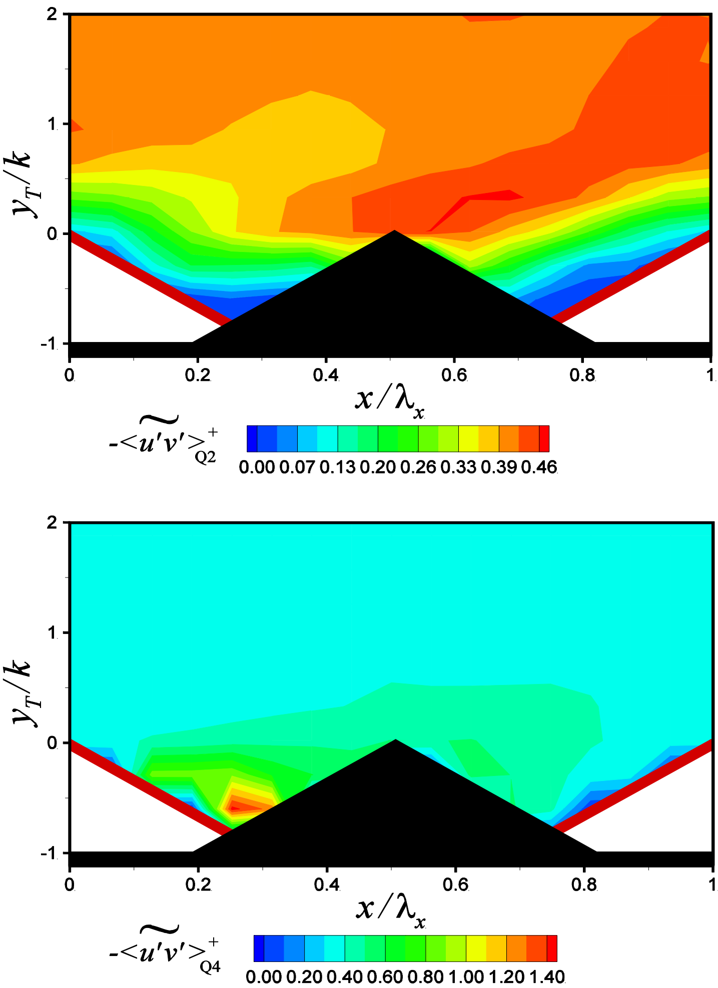

a)

b)

Fig.6 Contribution to the Reynolds shear stresses from a) Q2 events, b) Q4 events. *H*=1.

The contributions to the Reynolds shear stress from moderate-to-strong events (H=1) are shown in Figs.6a and 6b referring respectively to the case of ejections and sweep events. Far from the wall (1<y_T/k<2), $-<\widetilde{u'v'}>^{+}{}_{Q2}$ and $-<\widetilde{u'v'}>^{+}{}_{Q4}$ assume comparable values (about 0.4) with slightly higher values of $-<\widetilde{u'v'}>^{+}{}_{Q2}$. In the region near the top of the pyramids similar behavior of the Q2 and Q4 moderate-to-strong events can be observed. Both $-<\widetilde{u'v'}>^{+}{}_{Q2}$ and $-<\widetilde{u'v'}>^{+}{}_{Q4}$ show increasing values from $x/\lambda_x \cong 0$ to the region near the top of the sketched dark pyramid followed by decreasing values moving downstream. In particular, for y_T/k=0, $-<\widetilde{u'v'}>^{+}{}_{Q2}$ assumes a value around 0.12 close to the top of the pyramid and much higher values, around 0.45, for $x/\lambda_x \cong 0.5$. $-<\widetilde{u'v'}>^{+}{}_{Q4}$ assumes similar values as $-<\widetilde{u'v'}>^{+}{}_{Q2}$ at $x/\lambda_x \cong 0.5$ and y_T/k=0, while three times higher value can be observed in correspondence of the top of the pyramid. The very high value of $-<\widetilde{u'v'}>^{+} \cong 1.65$ (Fig. 4) in the downstream part of the pyramid, near the base, is mainly given by moderate-to-strong sweeps events.

The flow configurations during the dominant events (ejections and sweeps), obtained as result of the conditional averaging procedure based on the quadrant method, are shown in Figs. 7 and 8. The velocity field and the $u'v'$ correlation have been conditionally averaged on the base of moderate-to-strong (H=1) ejection events (Fig. 7) and moderate-to-strong sweep events (Fig. 8), both detected at x^+=50 (x/λ_x= 0.25) and y_T^+=-11 (y_T/k=-0.25), in the region of the downstream side of the pyramids, where a strong turbulence activity has been measured.

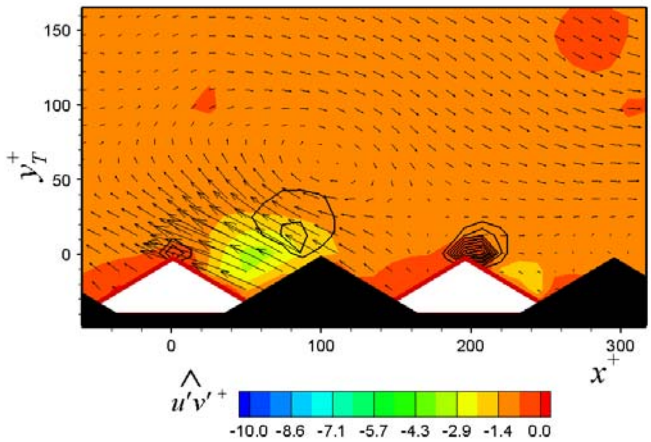

Fig.7 Ejection events detected at x^+=50 , y_T^+=-11 . H=1 . Colour map: conditionally averaged $u'v'$ correlation. Contour lines: conditionally averaged swirling strength isolines. Vectors: conditionally averaged fluctuating velocity field.

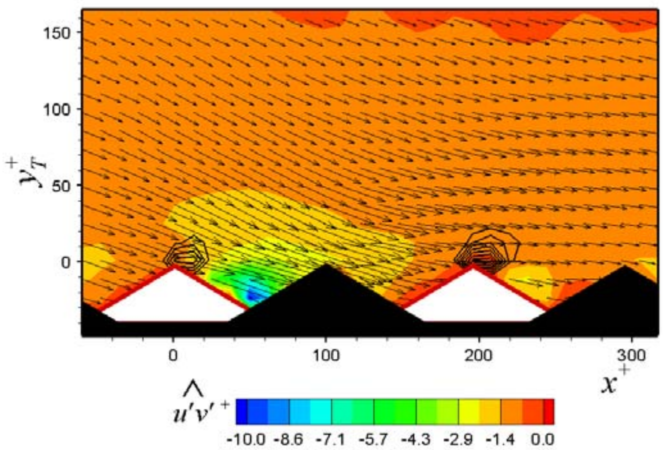

Fig.8 Sweep events detected at x^+=50 , y_T^+=-11 . H=1 . Colour map: conditionally averaged $u'v'$ correlation. Contour lines: conditionally averaged swirling strength isolines. Vectors: conditionally averaged fluctuating velocity field.

The colour map represents the conditionally averaged $u'v'$ correlation. The vectors are the conditionally averaged fluctuating velocity obtained using Reynolds decomposition. The continuous lines are swirling strength isolines, λ_{ci} = constant, computed on the conditionally averaged velocity field. Swirling motions at the top of the pyramids are highlighted in both figures. These observed swirling patterns can be tentatively interpreted as the result of two combined effects in the conditionally averaging process. The first effect is due to the transit of previously generated vortical structure travelling along the wall (see Fig.5), retarded and intensified when interacting with the flow around the roughness element. The second effect is related to the vortices locally originating from the interaction of the incoming flow with the pyramids and successively convected downstream. The last process can be associated to a specific near wall turbulence production mechanism in the roughness layer. In Fig.7 a further swirling motion just upstream the top of the sketched dark pyramid is clearly individuated by the swirling strength isolines, at about x^+=80 (x/λ_x= 0.4) and y_T^+=15 (y_T/k=0.3). The presence of this structure suggests that the conditionally averaged ejection event detected at x^+=50 (x/λ_x= 0.25) and y_T^+=-11 (y_T/k=-0.25) is mainly produced by this large scale clockwise swirling motion. It should be noted that the rotation centre of the circulation observed in the conditionally averaged fluctuating flow field does not coincide with the centre of the swirling motion detected by the λ_{ci} method. This discrepancy is due to the fact that the local conditionally averaged velocity after the Reynolds decomposition is different from the vortex convective velocity. It should be also noted in Fig. 7 that the vortex on the top of the upstream pyramid appears to be weaker than the one on the top of the downstream pyramid, due to an unwind effect related to the flow velocity induced by the swirling motion just upstream the top of the sketched dark pyramid. The conditionally averaged flow field relative to moderate-to-strong sweep events, detected at x^+=50 (x/λ_x= 0.25) and y_T^+=-11 (y_T/k=-0.25), is shown in Fig. 8. It appears to be due to the combination of the vortical flow at the top of the upstream pyramid and a large scale (with respect to the roughness element) inflow motion. Moreover, the very high value of the $u'v'$ correlation downstream the pyramid, near its base, depends also on the interaction of this flow motion with the wall geometry.

4 Conclusions

PIV measurements at relatively low Reynolds numbers in a turbulent boundary layer over a 3D-roughened surface, consisting of pyramidal rows, have been shown. Measurements have been taken in a streamwise wall normal plane intercepting the apex of a row of pyramids and the diagonal of the square base.

The results shown in the present paper point out the non-homogeneity of the flow in the roughness sub-layer. The different flow behaviour along the ascendant and the descendent part of the pyramids and in the region between two consecutive pyramids has been visualized. Low values of the streamwise component of the mean velocity and high values of the Reynolds shear stresses are present in the downstream part of the pyramids, near their base. It should be emphasized the high values (about 1.5) assumed in this region by the Reynolds shear stress. These values are much higher than the maximum value ($-<\widetilde{u'v'}>^+$ = 0.9) expected near the wall at the same Reynolds number in a smooth wall turbulent boundary layer.

The observation of instantaneous PIV images suggests that two series of vortical structures appear to be present. Vortices are seen to travel nearly parallel to the wall, very close to the top of the pyramids, retarded and intensified when interacting with the flow around the roughness element. Moreover, swirling patterns are sometimes seen to originate from the interaction of the incoming flow with the pyramids and successively are seen to be convected downstream. It is argued that this process can be associated with a specific near wall turbulence production mechanism in the roughness sub-layer. Farther from the wall, packets of vortical structures are seen having origin and behaviour similar to the one expected in a smooth wall turbulent boundary layer.

In order to understand the origin of the high turbulence activity observed downstream the pyramids, near their base, a classical quadrant analysis has been performed. Particularly, the flow events producing the high values of the Reynolds shear stress have been analyzed. The large values of $-<\widetilde{u'v'}>^{+}$, downstream the pyramids, near their base, are essentially due to sweep events, that give a contribution to the Reynolds shear stress about four times higher than the one from the ejections in the observed peak of $-<\widetilde{u'v'}>^{+}$.

The conditionally averaged analysis reveals that moderate-to-strong ejection events detected downstream the pyramids, near their base, are caused by the interaction of the flow induced by large scale clockwise vortical structures and the roughness geometry. The moderate-to-strong sweep events detected downstream the pyramids, near their base, are due to the combination of the vortical flow at the top of the pyramid and a large scale inflow motion. In addition, sweep events appear to be very efficient in contributing to the Reynolds shear stresses due to the favorable inclination of the roughness surface (the descendent part of the pyramid).

References

[1] Jiménez J. (2004) Turbulent flows over rough walls. *Ann. Rev. Fluid Mech.*, vol. 36, pp. 173-196.

[2] Flack K. A., Schultz M. P. (2014) Roughness effects on wall-bounded turbulent flows. *Phys. Fluids*, vol. 26, 101305.

[3] Djenidi L., Antonia R. A., Amielh M., and Anselmet F. (2008) A turbulent boundary layer over a two-dimensional rough wall. *Exp. Fluids*, vol. 44, 37-47.

[4] Vesely L., Haigermoser C., Greco D., Onorato M. (2009) Turbulent flow and organized motions over a two-dimensional rough wall. *Phys. Fluids*, vol. 21, 125107.

[5] Volino R. J., Schultz M. P., Flack K. A. (2011) Turbulence structure in boundary layers over periodic two- and three-dimensional roughness. *J. Fluid Mech.*, vol. 676, 172.

[6] Amir M., Castro I. P. (2011) Turbulence in rough-wall boundary layers: universality issues. *Exp. Fluids*, vol. 51, 313.

[7] Hong J., Katz J., Meneveau C., Schultz P. (2012) Coherent structures and associated subgrid-scale Energy transfer in a rough-wall turbulent channel flow. *J. Fluid Mech.*, vol. 712, 92-128.

[8] Schultz M. P., Flack K. A. (2009) Turbulent boundary layers on a systematically varied rough wall. *Phys. Fluids*, vol. 21, 015104.

[9] Hong J., Katz J., Schultz P. (2011) Near-wall turbulence statistics and flow structures over three-dimensional roughness in a turbulent channel flow. *J. Fluid Mech.*, vol. 667, pp. 1-37.

[10] Talapatra S., Katz J. (2012) Coherent structures in the inner part of a rough-wall channel flow resolved using holographic PIV. J. Fluid Mech., vol. 711, pp. 161-170.

[11] Perry A. E., Li J. D. (1990) Experimental support for the attached-eddy hypothesis in zero-pressure gradient turbulent boundary layers. J. Fluid Mech., vol. 218, pp. 405-438.

[12] Flack K. A., Schultz M. P., Connelly J. S. (2007) Examination of a critical roughness height for the outer layer similarity. *Phys. Fluids*, vol. 19, 095104.

[13] DeGraaff D. B., Eaton J. K. (2000) Reynolds-number scaling of the flat-plate turbulent boundary layer. *J. Fluid Mech.*, vol. 422, pp. 319-346.

[14] Zhou J., Adrian R. J., Balanchadar S., Kendal T. M. (1999) Mechanisms for generating coherent packets of hairpin vortices in channel flow. *J. Fluid Mech.*, vol. 387, pp. 353-396.

[15] Adrian R. J., Meinhart C. D., Tomkins C.D. (2000) Vortex organization in the outer region of the turbulent boundary layer. *J. Fluid Mech.,* vol. 422, pp. 1-54.

[16] Onorato M., Di Cicca G. M., Iuso G., Spazzini P. G., Malvano R. (2006) Turbulent boundary layers and

their control: Quantitative flow visualization results. Transition and turbulence control, Editors: Mohamed Gad-el-Hak and Her Mann Tsai. Institute for Mathematical Sciences, National University of Singapore.

[17] Liu Z., Adrian R. J., Hanratty T. J. (2001) Large scale modes of turbulent channel flow: transport and structure. *J. Fluid Mech.*, vol. 448, pp. 53-80.

[18] Christensen K. T., Adrian R. J. (2001) Statistical evidence of hairpin vortex packets in wall turbulence. *J. Fluid Mech.*, vol. 431, pp. 433-443.

[19] Lu S. S., Willmarth W. W. (1973) Measurements of the structure of the Reynolds stress in a turbulent boundary layer, *J. Fluid Mech.*, vol. 60, part 3, pp. 481-511.